

**Photometric Variability and Astrometric Stability
of the Radio Continuum Nucleus
in the Seyfert Galaxy NGC 5548**

J. M. Wrobel

National Radio Astronomy Observatory,
P.O. Box O, Socorro, New Mexico 87801
(e-mail: jwrobel@nrao.edu)

ABSTRACT

The NRAO VLA and VLBA were used from 1988 November to 1998 June to monitor the radio continuum counterpart to the optical broad line region (BLR) in the Seyfert galaxy NGC 5548. Photometric and astrometric observations were obtained at 21 epochs. The radio nucleus appeared resolved, so comparisons were limited to observations spanning 10-60 days and 3-4 yr, and acquired at matched resolutions of 1210 mas = 640 pc (9 VLA observations), 500 mas = 260 pc (9 VLA observations), or 2.3 mas = 1.2 pc (3 VLBA observations). The nucleus is photometrically variable at 8.4 GHz by $33 \pm 5\%$ and $52 \pm 5\%$ between VLA observations separated by 41 days and 4.1 yr, respectively. The 41-day changes are milder ($19 \pm 5\%$) at 4.9 GHz and exhibit an inverted spectrum ($\alpha \sim +0.3 \pm 0.1$, $S \propto \nu^{+\alpha}$) from 4.9 to 8.4 GHz. The nucleus is astrometrically stable at 8.4 GHz, to an accuracy of 28 mas = 15 pc between VLA observations separated by 4.1 yr and to an accuracy of 1.8 mas = 0.95 pc between VLBA observations separated by 3.1 yr. Such photometric variability and astrometric stability is consistent with a black hole being the ultimate energy source for the BLR, but is problematic for star cluster models that treat the BLR as a compact supernova remnant and, for NGC 5548, require a new supernova event every 1.7 yr within an effective radius $r_e = 42$ mas = 22 pc. A deep image at 8.4 GHz with resolution 660 mas = 350 pc was obtained by adding data from quiescent VLA observations. This image shows faint bipolar lobes straddling the radio nucleus and spanning 12 arcsec = 6.4 kpc. These synchrotron-emitting lobes could be driven by twin jets or a bipolar wind from the Seyfert 1 nucleus.

Subject headings: galaxies: individual (NGC 5548, UGC 09249) - galaxies: nuclei - galaxies: Seyfert - radio continuum: galaxies

1. Motivation

The Seyfert 1 galaxy NGC 5548 was the target of intensive space- and ground-based monitoring designed to measure the light travel time across its broad optical-line-emitting region

(Peterson 1993, Korista et al. 1995, and references therein). These reverberation studies imply that the broad line region (BLR) has a characteristic diameter $\lesssim 40$ light days, or $\leq 64 \mu\text{as}$ for $H_0 = 50 \text{ km s}^{-1} \text{ Mpc}^{-1}$ and the galaxy’s recession velocity relative to the 3 K background (5354 km s^{-1} ; de Vaucouleurs et al. 1991). Given this small size, is it possible to constrain models for the ultimate energy source for the BLR in NGC 5548? The common view is that the energy source is a supermassive black hole fuelled by an accretion disk (e.g., Peterson 1997), and three recent findings support this scenario for NGC 5548. First, analysis of variations in the emission line profiles of NGC 5548 suggests that the BLR material moves along randomly inclined Keplerian orbits defined by a central mass of order $\sim 7 \times 10^7 M_\odot$ (Wanders et al. 1995, Wanders & Peterson 1996, Peterson & Wandel 1999). Second, the central continuum source must irradiate the BLR anisotropically (Wanders et al. 1995, Wanders & Peterson 1996), perhaps because the continuum source is surrounded by an optically-thick accretion disk (cf. Figure 1 of Goad & Wanders 1996). Third, NGC 5548 exhibits very broad and asymmetric X-ray emission lines whose profiles are well matched by gravitationally-redshifted and fluorescing lines from accretion disk material (Nandra et al. 1997).

Still, the starburst hypothesis of Terlevich et al. (1992) potentially offers an alternative energy source: a compact star cluster hosts a supernova and the BLR is identified with the compact supernova remnant formed as the supernova ejecta interacts with dense circumstellar material. Although the star cluster hypothesis has yet to be tested against the three findings listed above for NGC 5548, it appears consistent with analysis of the optical continuum variability and the reverberation results (Aretxaga & Terlevich 1993, Terlevich et al. 1995). Astrometric monitoring of Seyfert nuclei offers another strong test of the starburst hypothesis (Melnick, Aretxaga, & Terlevich 1997). The low supernova rates and their short radiative lifetimes mean that as the compact star cluster evolves and new supernovae occur, the BLR should dance within the star cluster. In contrast, black hole models for low-power objects like Seyfert nuclei predict no motion of the nucleus over time, or simple linear motion if the emission arises from propagating shocks in a jet and counterjet (Falcke & Biermann 1996, Yi & Boughn 1998, Yi & Boughn 1999). This paper imposes observational constraints on the astrometric stability of the radio continuum nucleus of NGC 5548, to help distinguish between star cluster and black hole models for the energy source of the BLR. Although the star cluster models do not predict light curves for the radio continuum emission from a compact supernova remnant, Terlevich et al. (1995) do remark on the relevance of SN 1988Z to their models, as being an example of a (radio) supernova expanding into dense circumstellar material (Stathakis & Sadler 1991, Van Dyk et al. 1993). Therefore this paper also examines the photometric variability of the radio continuum nucleus of NGC 5548, for comparison with the photometric evolution of SN 1988Z at radio wavelengths.

2. Astrometric Imaging

Table 1 gives a log of the astrometric imaging observations of NGC 5548 with the Very Large Array (VLA, Thompson et al. 1980) and the Very Long Baseline Array (VLBA, Napier et al. 1994). Both instruments acquired data in dual circular polarizations at the center frequencies tabulated. For each polarization, the VLA bandwidth was 100 MHz with 3-level sampling and the VLBA bandwidth was 32 MHz with 4-level sampling. All VLA and VLBA observations after 1990 assumed a coordinate equinox of 2000. Earlier VLA observations assumed an equinox of 1950 and were transformed to 2000 using a reference date of 1979.9 for the phase calibrator grid used at the VLA prior to 1990 (Walker 1999).

On the VLA, an 8-minute observation of NGC 5548 was preceded and followed by an observation of the phase calibrator OQ 208 (B1404+286) about 4° from NGC 5548 (Figure 1). VLA observations of 3C 286 were used to set the amplitude scale to an accuracy of about 3%. On the VLBA, a 3-minute observation of NGC 5548 was preceded and followed by an observation of the phase, rate, and delay calibrator J1419+27 about 2° from NGC 5548 (Figure 1). The position assumed for J1419+27 was $\alpha_{J2000} = 14^h 19^m 59^s.29698$ and $\delta_{J2000} = +27^\circ 06' 25''.5540$, with an error in each coordinate of less than 1 mas (M. Eubanks, private communication). Sources OQ 208 and J1310+32 were also observed with the VLBA to check the astrometric accuracy and to align the phases of the baseband channels, respectively. VLBA system temperatures and gains were used to set the amplitude scale to an accuracy of about 5%, after first correcting for sampler errors. For both the VLA and VLBA, the position assumed for OQ 208 was $\alpha_{J2000} = 14^h 07^m 00^s.3943640$ and $\delta_{J2000} = +28^\circ 27' 14''.69129$ (M. Eubanks, private communication). These assumed positions for both J1419+27 (B1417+273) and OQ 208 agree with those in Ma et al. (1998). The VLA data were calibrated using the 1994 January 15 release of the NRAO AIPS software, while the VLBA data were calibrated with the 1999 April 15 release.

The AIPS task IMAGR was used to form and deconvolve images of the Stokes I emission from NGC 5548. Neither the VLA nor VLBA data on NGC 5548 were self-calibrated. The VLA images were made with a weighting scheme that achieved high angular resolution without seriously degrading sensitivity. Furthermore, VLA imaging tests showed that the peak source strength increased as angular resolution decreased, suggesting that the source was slightly resolved. Thus only VLA images with matched resolutions were analysed. The VLBA images were made with natural weighting to optimize sensitivity and were restored with a matched elliptical Gaussian beam. Photometric and astrometric comparisons will be limited to observations at matched angular resolutions of 500 mas = 260 pc (Figure 2, 9 VLA observations), 1210 mas = 640 pc (Figure 3, 9 VLA observations), and 2.3 mas = 1.2 pc (Figure 4, 3 VLBA observations).

Image rms values (σ_I) appear in Table 1 in units of microjanskys per beam area ($\mu\text{Jy ba}^{-1}$); all rms values match those expected given the array and observation parameters (Wrobel & Walker 1999). The image resolutions, expressed either as the FWHM dimension of a circular Gaussian beam or the FWHM dimensions and elongation orientation of an elliptical Gaussian beam, also

appear in Table 1. The tabulated position peaks were derived from quadratic fits in the image plane. For the VLA images, these quadratic fits also yielded the peak flux densities listed in the table, along with errors that are quadratic sums of a 3% scale error and σ_I . For the VLBA images, the source appeared to be resolved, so total flux densities were derived by integration over $N \sim 10$ beam areas and tabulated along with errors that are quadratic sums of a 5% scale error and $\sigma_I\sqrt{N}$. This apparent resolution could be due either to unmodelled atmospheric and/or station motion effects (Beasley & Conway 1995), or due to real structure. That the structure is similar in the VLBA images suggests the latter but does not prove it, because some phase-referencing errors can be systematic from observation to observation.

The table also notes the $1\sigma_A$ error in each coordinate for the astrometry of the peak position. σ_A is the quadratic sum of a term measuring the peak signal-to-noise ratio (Ball 1975) and a term measuring the accuracy of the absolute astrometry. This latter term was *estimated* in the VLA case as follows. The imaging at 500-mas resolution was done in the same configuration and season as Patnaik et al. (1992) or in the same configuration and contemporaneous with Browne et al. (1998). Those authors used phase calibrators 10° or less from their targets, cycled back to a calibrator every 6 minutes, and measured a 1-D positional accuracy of about 10 mas rms. The present work involves a calibrator 4° from the target (Figure 1) but observed with a 10-minute cycle time, so 20 mas was adopted as an estimate for the 1-D accuracy of the absolute VLA astrometry. In the VLBA case, the accuracy of the absolute astrometry was *derived* from analysis of the astrometric check source OQ 208, as referenced to J1419+27. As Figure 1 shows, OQ 208 and J1419+27 are separated by about 3° , while the separation between J1419+27 and NGC 5548 is about 2° . Thus the position error for OQ 208 as referenced to J1419+27, plotted in Figure 5, serves as a cautious upper limit to the position error for NGC 5548 as referenced to J1419+27. Indeed, residual position errors of order 1 mas and 0.7 mas are expected for separations of 3° and 2° , respectively, due to known deficiencies in the 1980 IAU nutation model adopted at the correlator (Ma et al. 1998).

3. Photometric Analysis

Photometric monitoring results from Table 1 are plotted in Figure 6. Each figure panel shows results for a given angular resolution within 100 days centered on the mean observation epoch indicated. Data at 8.4 GHz are plotted as dark symbols, while data at 4.9 GHz appear as light symbols. The figure legend indicates which symbols encode which matched angular resolutions. Photometric comparisons should only be made among data at matched resolutions. To aid such comparisons the pairs of panels at the top, middle, and bottom of Figure 6 show data at matched resolution, with the left columns having the earlier mean epoch of observation.

Figure 6 demonstrates that the radio nucleus of NGC 5548 is photometrically variable, on timescales that are both short (comparing within a panel) and long (comparing across paired panels). Specifically, the maximum flux densities are higher than minimum flux densities, by

$33 \pm 5\%$ between VLA observations separated by 41 days (panel [d]) and by $52 \pm 5\%$ between VLA observations separated by 4.1 yr (panel [a] *versus* [b]). Panel (d) also establishes that the 41-day “flare” is milder ($19 \pm 5\%$) at 4.9 GHz than at 8.4 GHz. Furthermore, the spectral index α ($S \propto \nu^{+\alpha}$) is $\alpha \sim -0.2 \pm 0.1$ prior to the 41-day “flare” but $\alpha \sim +0.3 \pm 0.1$ during the “flare”. Thus the “flare” is optically thick and milder at the lower frequency, traits typical for variable active nuclei. The “flare” is too poorly sampled to derive a meaningful variability timescale. The flux densities plotted in Figure 6 correspond to 8.4-GHz powers $P_\nu \sim 2.5 - 8.3 \times 10^{21}$ W Hz⁻¹, while the associated luminosities are $L_\nu = \nu P_\nu \sim 2.1 - 7.0 \times 10^{38}$ erg s⁻¹.

The radio sampling in Figure 6 is too coarse for useful comparisons with concurrent continuum monitoring from the ground or space. However, some relevant comparison can be made in connection with the 41-day radio variability between 1993 March 15 and April 25. First, that radio variability is much slower than the 1-day and 3-day variability reported for the hard and soft x-rays, respectively, during the period 1992 December to 1993 January (Done et al. 1995). Second, the 33% change during the 41-day radio “flare” is comparable to the 40% changes documented for the continuum at 5100Å during the period 1993 March 19 to May 27 (Korista et al. 1995).

3.1. Implications for Black Hole Models

Radio continuum emission can arise from (1) an advection-dominated accretion flow (ADAF) onto a black hole (Yi & Boughn 1998), (2) jets emerging from an ADAF (Yi & Boughn 1999), or (3) jets emerging from a standard accretion disk which itself emits no radio photons (Falcke & Biermann 1996). Comparisons with these models will assume a black hole mass $\sim 7 \times 10^7 M_\odot$ (Peterson & Wandel 1999) and will try to match the spectral indices α , luminosities L_ν , and photometric variability observed for the radio nucleus of NGC 5548, plus be consistent with VLBA emission being predominantly unresolved.

The radio continuum from an ADAF is synchrotron emission from an X-ray emitting and optically-thin plasma (Yi & Boughn 1998, Yi & Boughn 1999), and is characterized by three key traits. First, Equation 1 of Yi & Boughn (1999) predicts that the radio power should have an inverted spectral index $\alpha = +0.2$, consistent with the index measured in the “flaring” state ($\alpha \sim +0.3 \pm 0.1$) but not in the quiescent state ($\alpha \sim -0.2 \pm 0.1$). Second, Equation 2.7 of Yi & Boughn (1998) implies that the 8.4-GHz photons should originate about 6 Schwarzschild radii from the black hole, placing them at radii less than 0.1 μ as, which is consistent with the VLBA emission being predominantly unresolved. Finally, Equations 1 and 3 of Yi & Boughn (1999) predict an 8.4-GHz luminosity $L_\nu = \nu P_\nu \sim 7 \times 10^{36}$ erg s⁻¹. This is about 30 – 100 times weaker than observed and argues for an alternative source of radio photons. Radio emission from jets is a plausible alternative, but before turning to that topic the existing evidence for outflow from the nucleus of NGC 5548 will be described.

Figure 7 displays a VLA image at 8.4 GHz with resolution 660 mas = 350 pc and rms

sensitivity $\sigma_I = 12 \mu\text{Jy ba}^{-1}$. This deep image was obtained by adding the 1988-1989 VLA data lacking evidence for photometric variability (see panels [a] and [c] in Figure 6) and two further 1989 observations at lower resolution. Areal integration over the figure yields a total flux density of $8.5 \pm 0.3 \text{ mJy}$, corresponding to a total power at 8.4 GHz of $1.2 \times 10^{21} \text{ W Hz}^{-1}$. Figure 7 shows that bipolar lobes straddle the radio nucleus and span $12 \text{ arcsec} = 6.4 \text{ kpc}$. The lobes are very faint at 8.4 GHz, with peak intensities $< 160 \mu\text{Jy ba}^{-1}$. The lobe morphologies confirm previous hints from images at lower resolution (Figure 3, Wilson & Ulvestad 1982, Baum et al. 1993, Kukula et al. 1995, Nagar et al. 1999) that the southern lobe is amorphous and the northern lobe is edge-brightened, possibly due to a bubble-like structure in 3-D.

These synchrotron-emitting lobes could be driven by a bipolar wind emanating from the nucleus of NGC 5548, as has been suggested for NGC 3079 (Baan & Irwin 1995, Trotter et al. 1998). Models for the absorption of the X-ray and ultraviolet continuum from NGC 5548 do imply outflowing ionized gas on subparsec scales (Mathur, Elvis, & Wilkes 1995). The shape of the subparsec outflow (radial *versus* bipolar *versus* cylindrical) is not constrained, but its kinetic luminosity of $10^{43} \text{ erg s}^{-1}$ is four orders of magnitude higher than the photon luminosities of the radio lobes (Wilson & Ulvestad 1982). If the subparsec outflow contains relativistic plasma, then Figure 4 could be used to trace the shape of the flow on parsec scales provided the reality of the apparent VLBA structure was verified (see Section 2). It is worth noting that weak synchrotron emission from relativistic plasma on scales 100-500 pc could be responsible for the source resolution effects, discussed in Section 2, that prompted the use of matched angular resolutions.

Suppose the synchrotron luminosity of the jets on scales $\lesssim 500 \text{ pc}$ is powered by a rotating black hole accreting from a magnetized plasma. Then the jet luminosity can be estimated from the Blandford-Znajek process given values for the spin parameter $\bar{a} \leq 1$ of the black hole, the efficiency $\epsilon_{\text{jet}} \leq 1$ of the jet radio emission, and the mass accretion rate \dot{m} , normalized to the Eddington rate (Yi & Boughn 1999). Adopting \dot{m} from an ADAF analysis of NGC 5548 leads to radio jet luminosities of $L_\nu \sim 8.4 \times 10^{43} \bar{a}^2 \epsilon_{\text{jet}} \text{ erg s}^{-1}$. This process could easily match the required radio jet luminosities on scales $\lesssim 500 \text{ pc}$, but the predictions are woefully imprecise compared to the predictions from the ADAF models. This process could also in principal match the kinetic luminosity of $10^{43} \text{ erg s}^{-1}$ for the subparsec outflow (Mathur, Elvis, & Wilkes 1995). Alternatively, in the jet-disk symbiosis model of Falcke & Biermann (1996), the radio jet luminosity and the (standard) accretion disk luminosity are correlated. Gauging the latter for NGC 5548 by the nuclear bolometric luminosity of $5 \times 10^{44} \text{ erg s}^{-1}$ (Mathur, Elvis, & Wilkes 1995), then the radio jet luminosity is as expected from that jet/disk correlation. Moreover, the spectral index of the quiescent radio emission is as expected for an inhomogeneous jet model, while the inverted spectrum during the 41-day “flare” could arise from a brightening in the optically-thick base of the jet.

3.2. Implications for Star Cluster Models

Terlevich et al. (1995) note the relevance of SN 1988Z to their models, as being an example of a (radio) supernova expanding into dense circumstellar material (Stathakis & Sadler 1991). It is thus of interest to compare the radio properties of this most distant known radio supernova (Van Dyk et al. 1993), with those of the radio nucleus in NGC 5548. Van Dyk et al. (1993) conclude that SN 1988Z is a rare, peculiar Type II supernova, which represents the endpoint of stellar evolution for a massive progenitor ($\sim 20 - 30 M_{\odot}$) that underwent a period of high mass loss ($\gtrsim 10^{-4} M_{\odot} \text{ yr}^{-1}$) before explosion. SN 1988Z achieved a maximum power at 8.4 GHz of about $2 \times 10^{21} \text{ W Hz}^{-1}$, similar to the minimum power recorded in Figure 6 for the radio nucleus of NGC 5548. Van Dyk et al. (1993) present models quantifying the photometric evolution of SN 1988Z at 8 and 5 GHz. (While the evolution appears to be smooth, the defining light curves are not well sampled in time.) Their models are plotted in Figure 8 with an arbitrary epoch shift for comparison with the VLA data from panel (d) of Figure 6. The radio supernova models appear able to account for the photometric variability of NGC 5548 observed on time scales of years. Those models cannot, however, account for the variability observed on time scales of tens of days.

4. Astrometric Analysis

All astrometric monitoring results from Table 1 are plotted in Figure 9. Each panel shows data at the matched angular resolution indicated, with the panels ordered as in Figure 6 to aid astrometric comparisons among data at matched resolutions. The origin for each panel is taken to be the position of the nucleus measured from the VLBA image at epoch 1995.337. Data at 8.4 GHz are plotted as dark symbols, while data at 4.9 GHz appear as light symbols. The symbol shapes encode the matched angular resolution and have the same meaning as in Figure 6.

Figure 9 implies that the radio nucleus of NGC 5548 is astrometrically stable, on timescales that are both short (comparing within a panel) and long (comparing across paired panels). Panels (a) and (b) demonstrate that the nucleus is astrometrically stable at 8.4 GHz, to an accuracy of $20\sqrt{2} \text{ mas} = 28 \text{ mas} = 15 \text{ pc}$ between VLA observations spanning both tens of days and 4.1 yr. Panels (c) and (d) verify this stability but with a poorer accuracy of $25\sqrt{2} \text{ mas} = 35 \text{ mas} = 19 \text{ pc}$. The nucleus is as astrometrically stable at 4.9 GHz as it is at 8.4 GHz, based on comparisons within panels (b) and (d). Finally, panels (e) and (f) imply that the nucleus is astrometrically stable at 8.4 GHz, to an accuracy of $1.3\sqrt{2} \text{ mas} = 1.8 \text{ mas} = 0.95 \text{ pc}$ between VLBA observations spanning 13 days and 3.1 yr.

4.1. Implications for Black Hole Models

The observed astrometric stability is consistent with any models based on black holes, including ADAF and jet models, but an ADAF model was ruled out photometrically in Section 3.1. If the reality of the apparent VLBA structure in Figure 4 could be verified, then those images could be used to constrain the evolution of the lengths of, or features within, any jets or counterjets. Furthermore, if a VLBA image was acquired during a radio flare, then the peak in that image would arise from the optically-thick base of the jet and would be expected to be located closer to the black hole.

4.2. Implications for Star Cluster Models

Suppose that the blue luminosity from the Seyfert “nucleus” of the NGC 5548 arises from a compact star cluster. Then the absolute magnitude of the cluster can be equated to the historical minimum of $M_B = -20.6$ mag recorded for the Seyfert nucleus (Aretxaga & Terlevich 1993). A star cluster with that magnitude will be characterized by an optical supernova rate of 0.6 yr^{-1} (Aretxaga & Terlevich 1994) and an effective radius $r_e = 22 \text{ pc} = 42 \text{ mas}$ (Young 1976, Melnick, Aretxaga, & Terlevich 1997). Each new optical supernova event should yield a radio counterpart if SN 1988Z is indeed as relevant to the starburst models as claimed by Terlevich et al. (1995).

A circle with the effective radius r_e of the star cluster is shown in panels (a)-(d) in Figure 9, with the circle arbitrarily centered at the origin. Figure 9 implies that radio nucleus of NGC 5548 does not move with the characteristic step size r_e between supernova events, as predicted by Melnick et al. (1997). The strongest constraints follow from the VLBA-VLBA astrometric stability at the 1-pc level for observations separated by 3.1 yr. However, in the star cluster model it is the massive stars which are the supernova progenitors, so if the initial mass function is biased toward massive stars and/or mass segregation is occurring, then the radio supernova would occur within a region of radius much smaller than $r_e = 22 \text{ pc} = 42 \text{ mas}$ (Melnick, Aretxaga, & Terlevich 1997).

The optical supernova rate of 0.6 yr^{-1} for NGC 5548 is moderately high, leading to a new supernova event about every 1.7 yr. This motivates a deep search for secondary radio sources at the matched VLBA resolution. Data from VLBA epochs 1998.445 and 1998.481 were combined to yield an image with rms $\sigma_I = 41 \mu\text{Jy ba}^{-1}$, corresponding to about 100 times the strength of Casseopia A were it placed at the distance of NGC 5548 (Baars et al. 1977). No secondary sources stronger than $5\sigma_I$, or about 200 times Casseopia A, were found in about 7600 VLBA beam areas within an annular region, centered as for Figure 9 and with inner radius $10 \text{ mas} = 5.3 \text{ pc}$ and outer radius $84 \text{ mas} = 45 \text{ pc} = 2r_e$. This outer radius is well within the limitations to the field of view given the VLBA observing strategies (Wrobel 1995). The absence of secondary VLBA sources, in conjunction with the VLBA constraints on the astrometric stability of the radio source, requires the presence of no more than one radio supernova during a 3.1-yr interval. This condition is improbable if the detected VLBA source really is a radio supernova whose slow decline, based

on the VLBA photometry, is shared by other radio supernovae. Thus either the radio supernova rate is lower than 0.6 yr^{-1} and/or, as mentioned above, the radio supernovae occur within a region of radius much smaller than $r_e = 22 \text{ pc} = 42 \text{ mas}$.

5. Conclusions and Future

The VLA and VLBA were used to monitor the radio continuum counterpart to the optical broad line region (BLR) in the Seyfert galaxy NGC 5548. The nucleus is photometrically variable at 8.4 GHz by $33 \pm 5\%$ and $52 \pm 5\%$ between VLA observations separated by 41 days and 4.1 yr, respectively. The 41-day changes are less pronounced ($19 \pm 5\%$) at 4.9 GHz and exhibit an inverted spectrum ($\alpha \sim +0.3 \pm 0.1$, $S \propto \nu^{+\alpha}$) from 4.9 to 8.4 GHz. The nucleus is astrometrically stable at 8.4 GHz, to an accuracy of 15 pc between VLA observations separated by 4.1 yr and to an accuracy of 0.95 pc between VLBA observations separated by 3.1 yr.

The photometric variability and astrometric stability of the radio nucleus is not consistent with star cluster models that treat the BLR as a compact supernova remnant and, for NGC 5548, required a new supernova event like SN 1988Z every 1.7 yr within an effective radius $r_e = 22 \text{ pc}$. The radio supernova models for SN 1988Z cannot account for the VLA variability observed on time scales of tens of days. The combined VLBA evidence for astrometric stability, no secondary sources, and slow photometric evolution of the detected source mean that the radio supernova rate is lower than predicted and/or the radio supernovae occur within a region much smaller than predicted. Additional VLBA monitoring would thus be beneficial, to provide further astrometric and photometric constraints on the detected radio source and to continue searches for secondary sources.

The photometric variability and astrometric stability of the radio nucleus in NGC 5548 is consistent with models of jets on scales $\lesssim 500 \text{ pc}$ emerging from a black hole. If the subparsec outflow inferred from X-ray/UV absorber models contains relativistic plasma, then the VLBA images could be used to trace the shape of the flow on parsec scales. However, the reality of the apparent VLBA structure must first be verified. Tracing flow kinematics to 100 pc should also be feasible through an HST study of the narrow optical emission lines, because those lines are so dominated by gas within $70 \text{ pc} = 130 \text{ mas}$ from the nucleus (Kraemer et al. 1998 and references therein).

A deep image at 8.4 GHz with a resolution 350 pc was obtained by adding data from quiescent VLA observations. This image shows faint bipolar lobes straddling the radio nucleus and spanning 6.4 kpc. The northern lobe is edge-brightened, suggesting a bubble-like structure in 3-D. These lobes are plausibly driven by twin jets or a bipolar wind from the Seyfert 1 nucleus. The kinematics of the flow could be followed to kiloparsec scales if neutral or molecular gas was detected in absorption against the radio continuum lobes. Sensitive polarimetry of the radio lobes could also constrain the properties of an enveloping magnetoionic medium and the topology of the

magnetic field in a synchrotron-emitting bubble.

The author thanks Dr. M. Eubanks for providing VLBI source positions; thanks Drs. J. Conway, R. Terlevich, J. Ulvestad and C. Walker for discussions; and acknowledges support from a SERC Visiting Fellowship held at Nuffield Radio Astronomy Laboratories, England. NRAO is a facility of the National Science Foundation operated under cooperative agreement by Associated Universities, Inc.

REFERENCES

- Aretxaga, I., & Terlevich, R. 1993, *Ap&SS*, 205, 69
- Aretxaga, I., & Terlevich, R. 1994, *MNRAS*, 269, 462
- Ball, J. A. 1975, in *Methods in Computational Physics, Volume 14*, eds. B. Alder, S. Fernbach, & M. Rotenberg (New York: Academic Press), 177
- Baan, W. A., & Irwin, J. A. 1995, *ApJ*, 446, 602
- Baars, J. W. M., Genzel, R., Pauliny-Toth, I. I. K., & Witzel, A. 1977, *A&A*, 61, 99
- Baum, S. A., O’Dea, C. P., Dallacassa, D., de Bruyn, A. G., & Pedlar, A. 1993, *ApJ*, 419, 553
- Beasley, A. J., & Conway, J. E. 1995, in *ASP Conf. Ser. 82, Very Long Baseline Interferometry and the VLBA*, eds. J. A. Zensus, P. J. Diamond, & P. J. Napier (San Francisco: ASP), 327
- Browne, I. W. A., Patnaik, A. R., Wilkinson, P. N., & Wrobel, J. M. 1998, *MNRAS*, 293, 257
- de Vaucouleurs, G., de Vaucouleurs, A., Corwin, H. G., Jr., Buta, R. J., Paturel, G., & Fouque, P. 1991, *Third Reference Catalog of Bright Galaxies* (New York: Springer)
- Done, C., Pounds, K. A., Nandra, K., & Fabian, A. C. 1995, *MNRAS*, 275, 417
- Falcke, H., & Biermann, P. 1996, *A&A*, 308, 321
- Goad, M., & Wanders, I. 1996, *ApJ*, 469, 113
- Korista, K. T. et al. 1995, *ApJS*, 97, 285
- Kraemer, S. B., Crenshaw, D. M., Filippenko, A. V., & Peterson, B. M. 1998, *ApJ*, 499, 719
- Kukula, M. J., Pedlar, A., Baum, S. A., & O’Dea, C. P. 1995, *MNRAS*, 276, 1262
- Ma, C., et al. 1998, *AJ*, 116, 516
- Mathur, S., Elvis, M., & Wilkes, B. 1995, *ApJ*, 452, 230
- Melnick, J., Aretxaga, I., & Terlevich, R. 1997, in *Science with the VLT Interferometer*, ed. F. Paresce (Berlin: Springer), 112
- Nagar, N. M., Wilson, A. S., Mulchaey, J. S., & Gallimore, J. S. 1999, *ApJS*, 120, 209
- Nandra, K., George, I. M., Mushotzky, R. F., Turner, T. J., & Yaqoob, T. 1997, *ApJ*, 477, 602
- Napier, P. J., Bagri, D. S., Clark, B. G., Rogers, A. E. E., Romney, J. D., Thompson, A. R., & Walker, R. C. 1994, *Proc. IEEE*, 82, 658
- Patnaik, A. R., Browne, I. W. A., Wilkinson, P. N., & Wrobel, J. M. 1992, *MNRAS*, 254, 655

- Peterson, B. M. 1993, *PASP*, 105, 247
- Peterson, B. M. 1997, *An Introduction to Active Galactic Nuclei* (Cambridge: CUP)
- Peterson, B. M., & Wandel, A. 1999, *ApJ*, 521, L95
- Stathakis, R. A., & Sadler, E.M. 1991, *MNRAS*, 250, 786
- Terlevich, R., Tenorio-Tagle, G., Franco, J., & Melnick, J. 1992, *MNRAS*, 255, 713
- Terlevich, R., Tenorio-Tagle, G., Rozyczka, M., Franco, J., & Melnick, J. 1992, *MNRAS*, 272, 198
- Thompson, A. R., Clark, B. G., Wade, C. M., Napier, P. J., 1980, *ApJS*, 44, 151
- Trotter, A. S., Greenhill, L. J., Moran, J. M., Reid, M. J., Irwin, J. A., & Lo, K. Y. 1998, *ApJ*, 495, 740
- Van Dyk, S. D., Weiler, K. W., Sramek, R. A., & Panagia, N. 1993, *ApJ*, 419, L69
- Walker, R. C. 1999, *The SCHED User Manual*, NRAO user document
- Wanders, I. et al. 1995, *ApJ*, 453, L87
- Wanders, I., & Peterson, B. M. 1996, *ApJ*, 466,174
- Wilson, A. S., & Ulvestad, J. S. 1982, *ApJ*, 260, 56
- Wrobel, J. M. 1995, in *ASP Conf. Ser. 82, Very Long Baseline Interferometry and the VLBA*, eds. J. A. Zensus, P. J. Diamond, & P. J. Napier (San Francisco: ASP), 413
- Wrobel, J. M., & Walker, R. C. 1999, in *ASP Conf. Ser. 180, Synthesis Imaging in Radio Astronomy II*, eds. G. B. Taylor, C. L. Carilli, & R. A. Perley (San Francisco: ASP), 171
- Yi, I., & Boughn, S. P. 1998, *ApJ*, 499, 198
- Yi, I., & Boughn, S. P. 1999, *ApJ*, 515, 576
- Young, P. J. 1976, *AJ*, 81, 807

Fig. 1.— Phase reference sources near NGC 5548.

Fig. 2.— Montage of VLA images of Stokes I emission from NGC 5548 at a matched resolution of $500 \text{ mas} = 260 \text{ pc}$ (hatched circle). Contours are at intervals of $2^{\frac{1}{2}}$ times the bottom contour level (BCL). Negative contours are dashed and positive ones are solid. Image peaks appear in Table 1. *Upper row:* Frequency 8.4 GHz. $BCL = 100 \mu\text{Jy ba}^{-1}$. Epochs left to right are 1988.913, 1988.989, 1989.036, and 1989.077. *Middle row:* Frequency 8.4 GHz. $BCL = 150 \mu\text{Jy ba}^{-1}$. Epochs left to right are 1992.814, 1992.858, 1992.891, 992.997, and 1993.025. *Bottom row:* Frequency 4.9 GHz. $BCL = 150 \mu\text{Jy ba}^{-1}$. Epochs left to right are as for the middle row.

Fig. 3.— Montage of VLA images of Stokes I emission from NGC 5548 at a matched resolution of $1210 \text{ mas} = 640 \text{ pc}$ (hatched circle). Contours are at intervals of $2^{\frac{1}{2}}$ times the bottom contour level (BCL). Negative contours are dashed and positive ones are solid. Image peaks appear in Table 1. *Upper row:* Frequency 8.4 GHz. $BCL = 100 \mu\text{Jy ba}^{-1}$. Epochs left to right are 1989.184, 1989.230, 1989.279, and 1989.318. *Middle row:* Frequency 8.4 GHz. $BCL = 150 \mu\text{Jy ba}^{-1}$. Epochs left to right are 1993.162, 1993.203, 1993.249, 1993.277, and 1993.315. *Bottom row:* Frequency 4.9 GHz. $BCL = 150 \mu\text{Jy ba}^{-1}$. Epochs left to right are as for the middle row.

Fig. 4.— Montage of VLBA images of Stokes I emission from NGC 5548 at a frequency of 8.4 GHz and a matched resolution of $2.3 \text{ mas} \times 1.1 \text{ mas} = 1.2 \text{ pc} \times 0.58 \text{ pc}$ (hatched ellipse). Contours are at intervals of $2^{\frac{1}{2}}$ times the bottom contour level of $150 \mu\text{Jy ba}^{-1}$. Negative contours are dashed and positive ones are solid. Total flux densities appear in Table 1. *Left:* Peak 1.93 mJy ba^{-1} . Epoch 1995.337. *Middle:* Peak 1.09 mJy ba^{-1} . Epoch 1998.445. *Right:* Peak 0.73 mJy ba^{-1} . Epoch 1998.481.

Fig. 5.— Observed minus expected VLBA position for OQ 208 at UT epochs 1995.337, 1998.445, and 1998.481.

Fig. 6.— Photometric monitoring of the radio continuum nucleus of NGC 5548 at the matched angular resolutions and mean epochs indicated. Data are from Table 1. Small circles and squares symbolize peak flux densities at a resolution of $500 \text{ mas} = 260 \text{ pc}$ (see Figure 2). Big circles and squares indicate peak flux densities at a resolution of $1210 \text{ mas} = 640 \text{ pc}$ (see Figure 3). Small diamonds correspond to integrated flux densities at a resolution of $2.3 \text{ mas} = 1.2 \text{ pc}$ times $1.1 \text{ mas} = 0.58 \text{ pc}$ (see Figure 4).

Fig. 7.— Deep VLA image of Stokes I emission from NGC 5548 at a frequency of 8.4 GHz, resolution of $660 \text{ mas} = 350 \text{ pc}$ (hatched circle), and a mean epoch of 1989.192. Contour levels are at intervals of $2^{\frac{1}{2}}$ times the bottom contour level, which is $30 \mu\text{Jy ba}^{-1}$. Negative contours are dashed and positive ones are solid. Grey scale ranges linearly from 30 to $180 \mu\text{Jy ba}^{-1}$.

Fig. 8.— Photometric monitoring of the radio continuum nucleus of NGC 5548 during the 41-day “flare”, for comparison with models for the photometric evolution of the radio supernova SN 1988Z.

Fig. 9.— Astrometric monitoring of the radio continuum nucleus of NGC 5548 at the matched angular resolutions and mean epochs indicated. Data are from Table 1. Symbols have the same meaning as in Figure 6. Section 4.2 describes the significance for the star cluster models of the circle in panels (a)-(d).

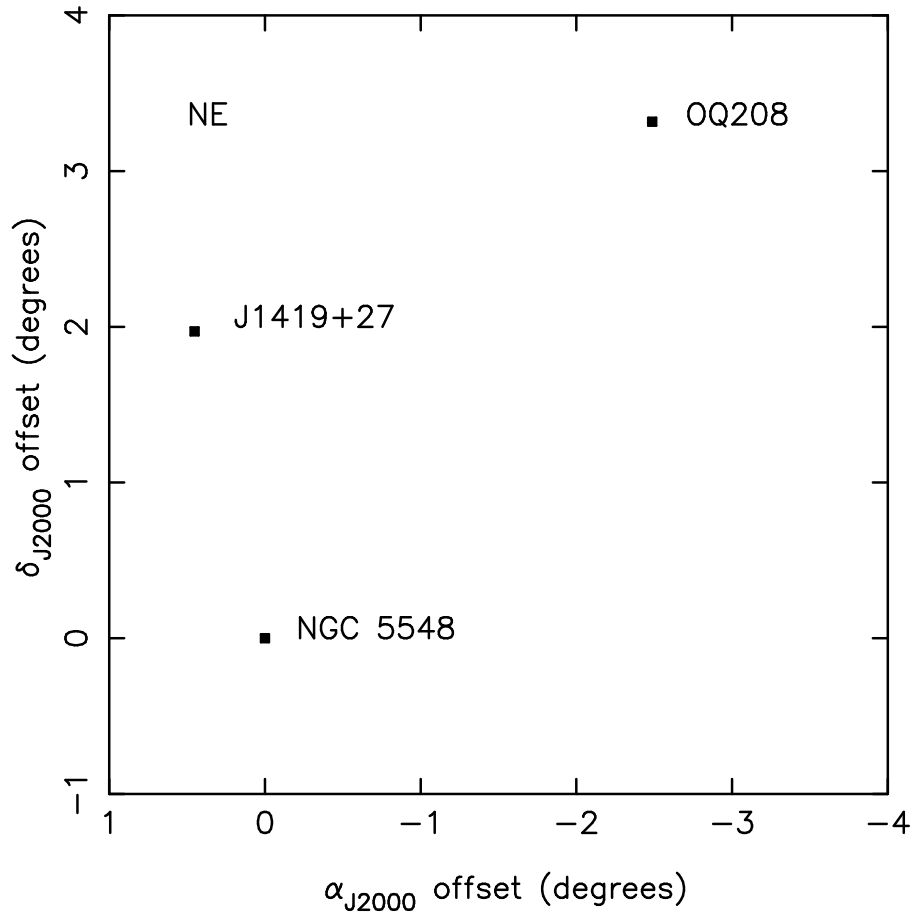


Figure 1

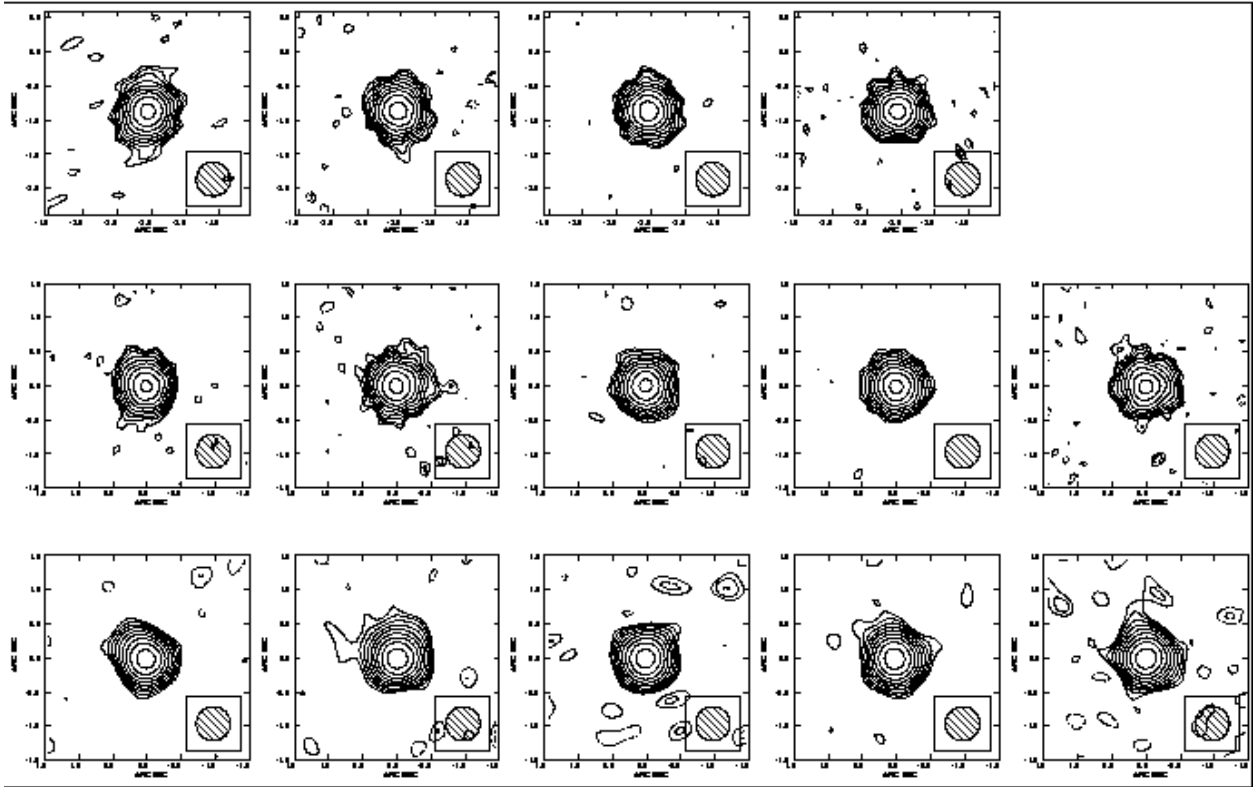


Figure 2

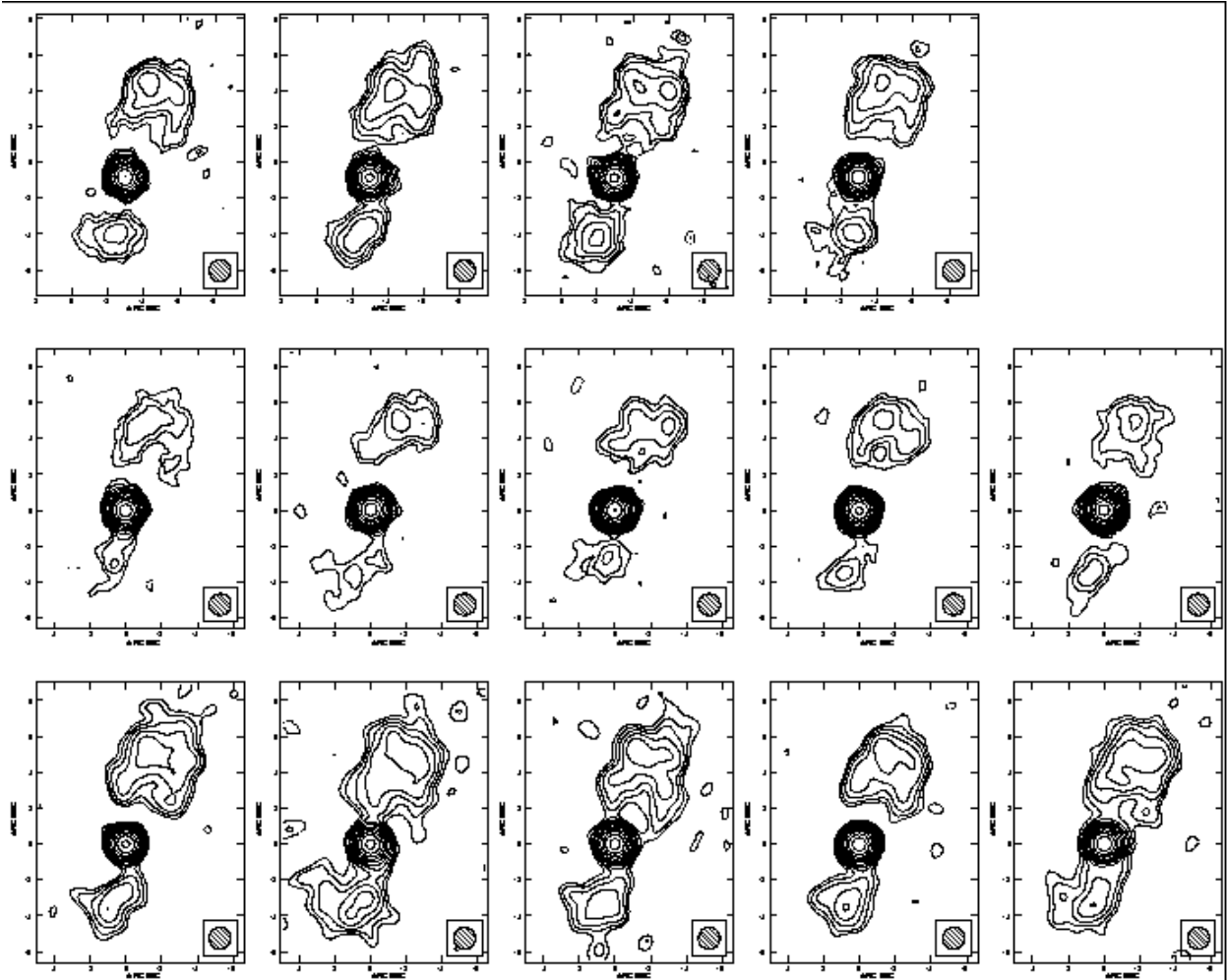


Figure 3

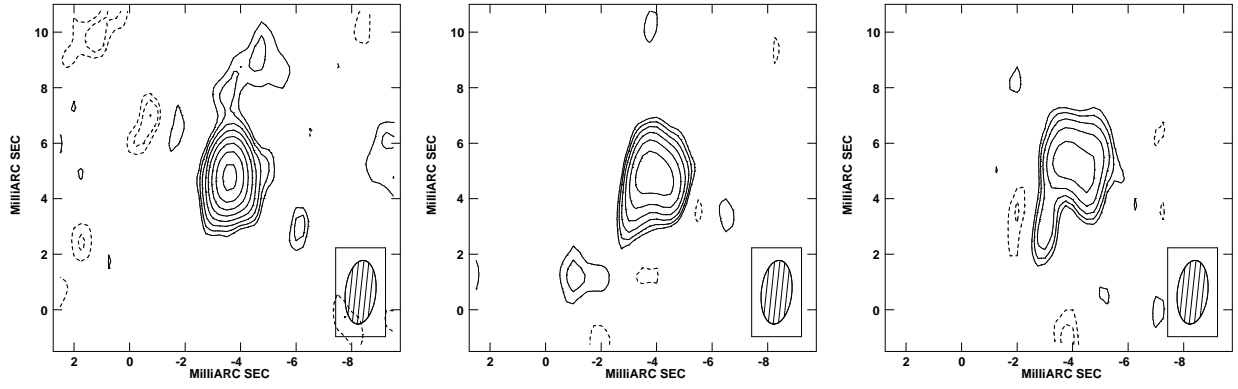


Figure 4

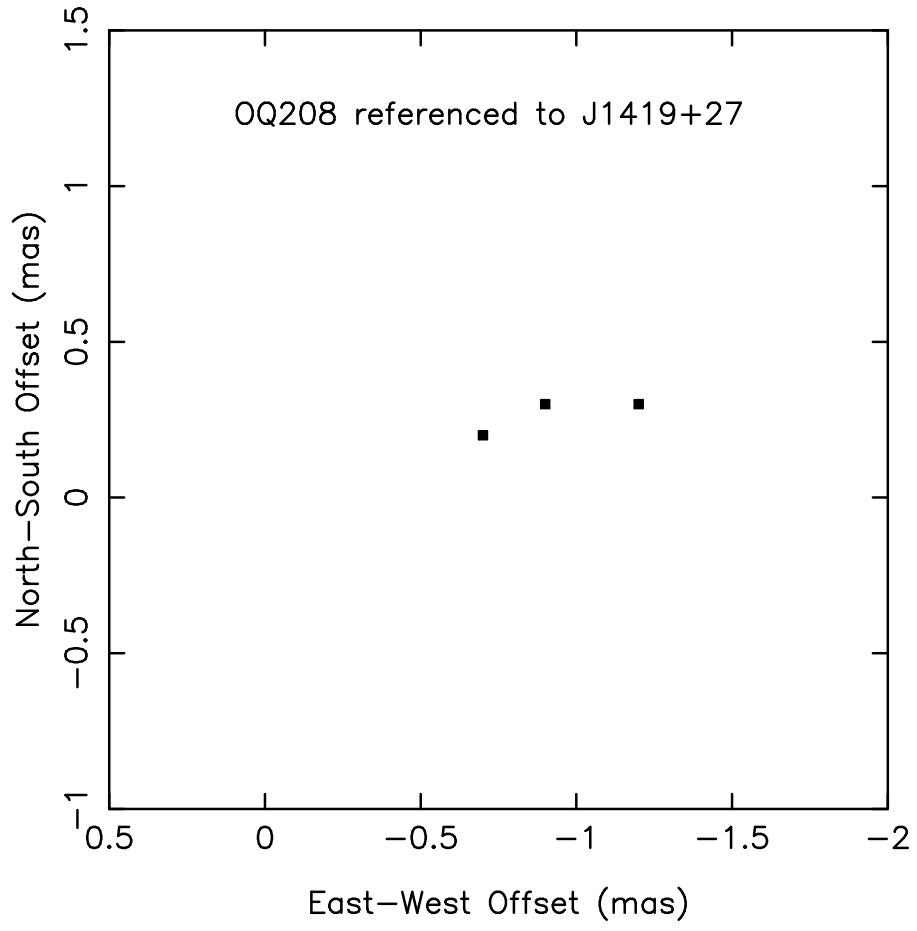


Figure 5

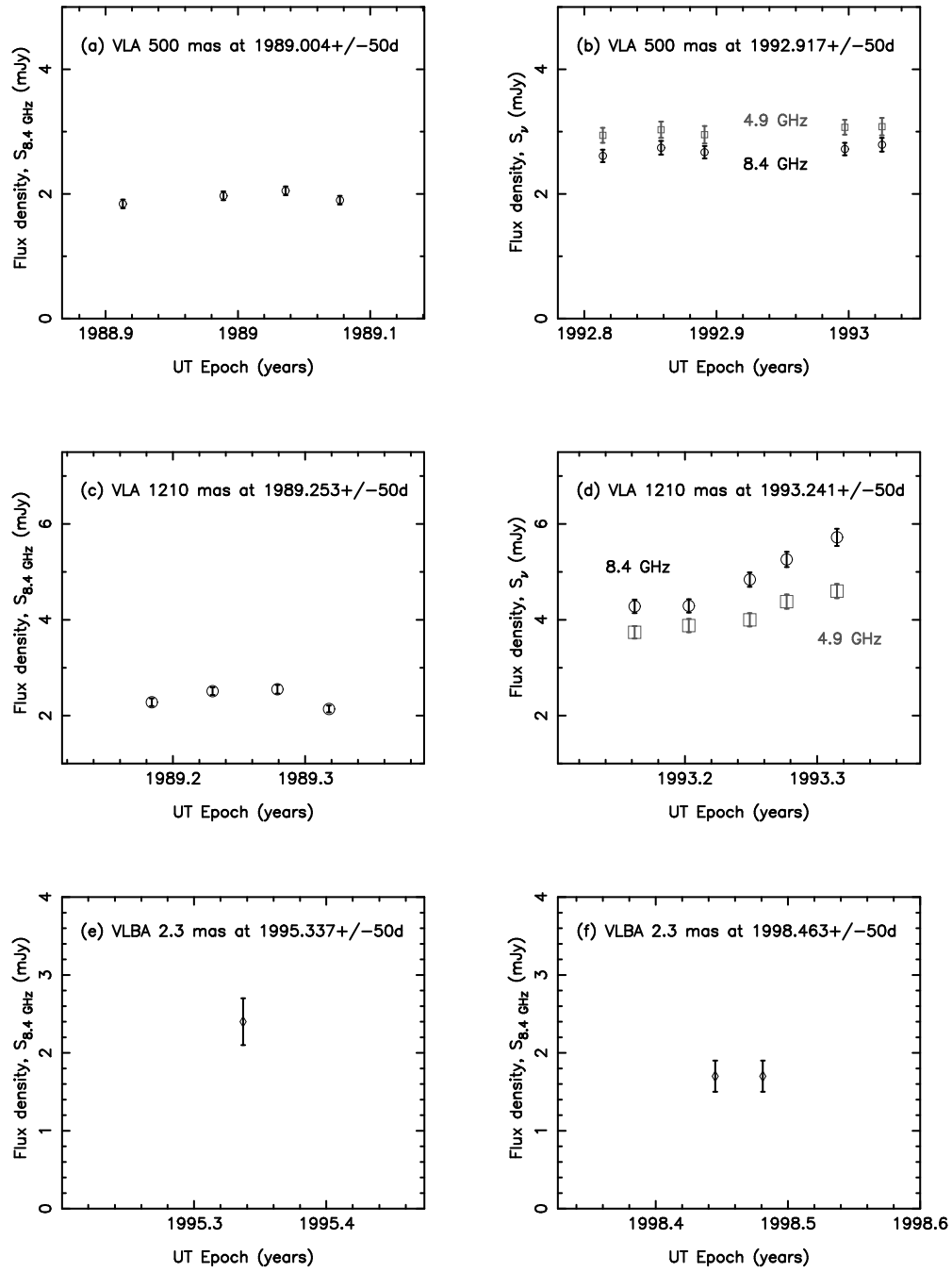


Figure 6

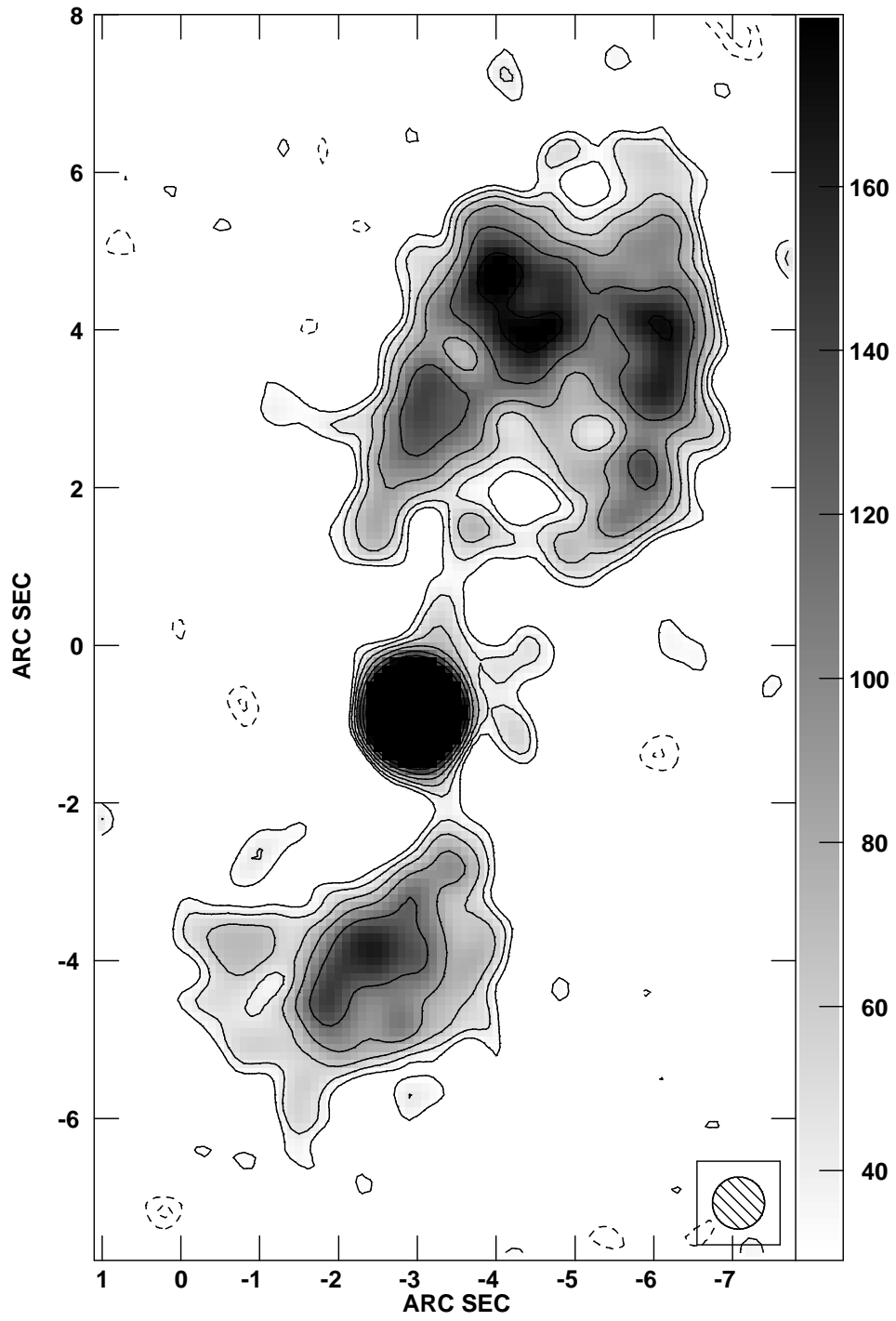


Figure 7

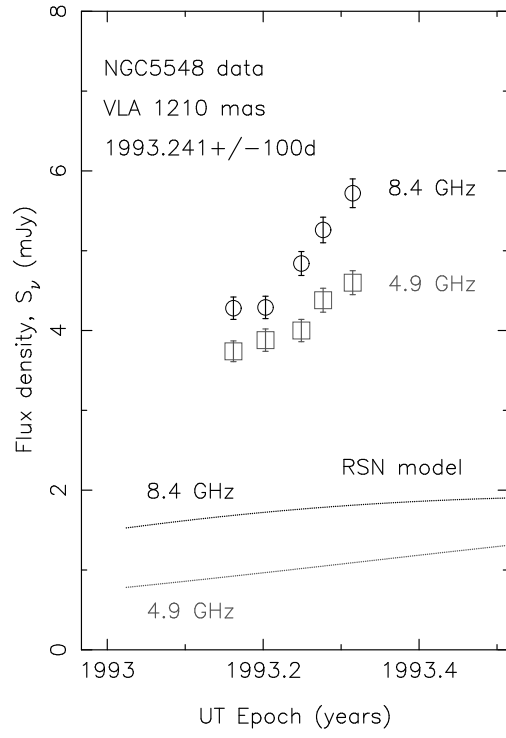


Figure 8

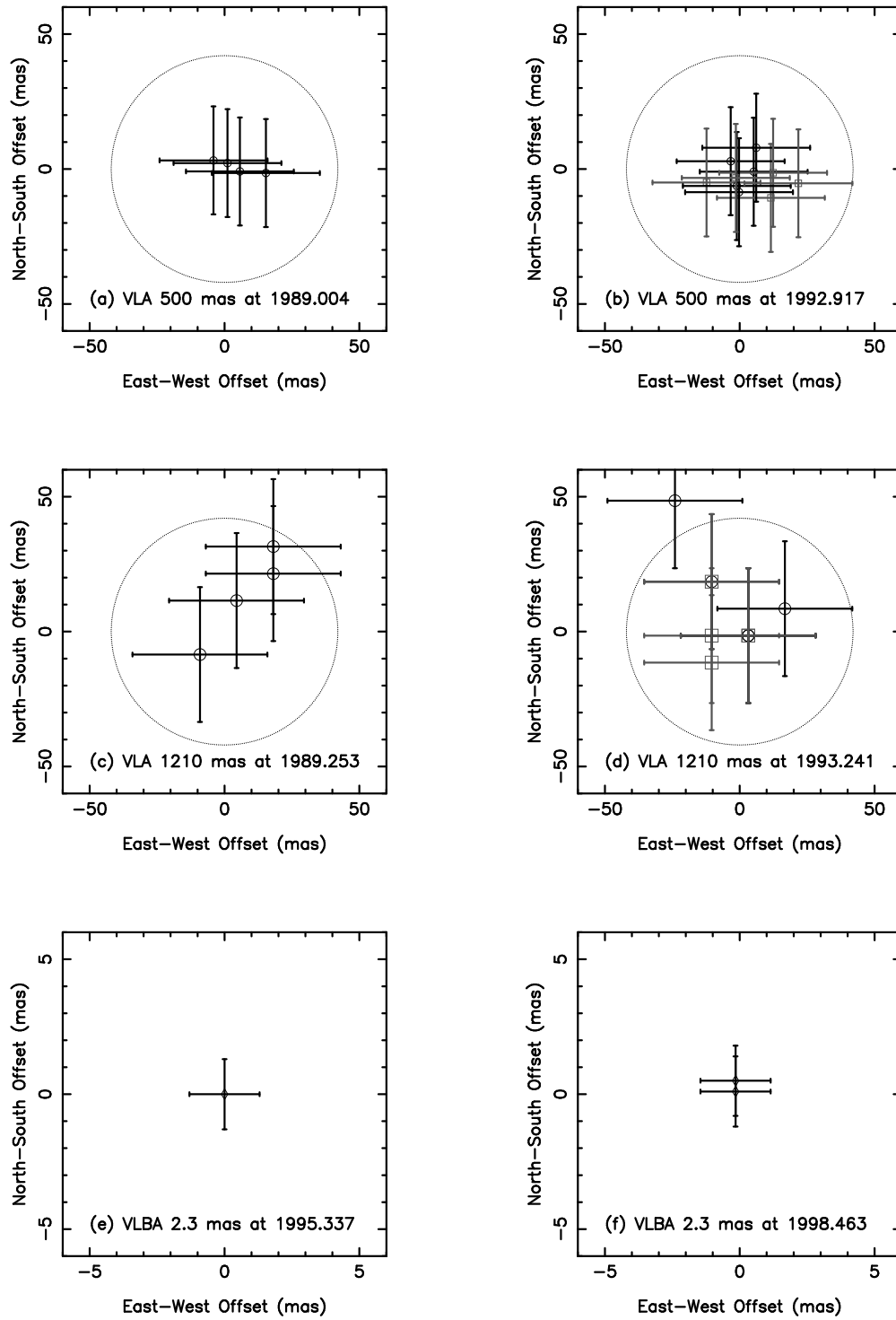


Figure 9

Table 1. Photometric and Astrometric Monitoring

UT Epoch	Array	Resolution (mas)	Freq. (GHz)	σ_I ($\mu\text{Jy ba}^{-1}$)	Peak α_{J2000}	Position δ_{J2000}	σ_A (mas)	Flux Density
1992.814 ...	VLA	500	8.4	75	14 ^h 17 ^m 59 ^s .5401	+25°08′12″.604	20	2.61 ± 0.11 ^a
1988.913 ...	VLA	500	8.4	43	14 17 59.5409	+25 08 12.603	20	1.84±0.07 ^a
1988.989 ...	VLA	500	8.4	44	14 17 59.5398	+25 08 12.607	20	1.97±0.07 ^a
1989.036 ...	VLA	500	8.4	36	14 17 59.5394	+25 08 12.608	20	2.05±0.07 ^a
1989.077 ...	VLA	500	8.4	44	14 17 59.5402	+25 08 12.604	20	1.90±0.07 ^a
1989.184 ...	VLA	1210	8.4	37	14 17 59.5411	+25 08 12.626	25	2.28±0.08 ^a
1989.230 ...	VLA	1210	8.4	33	14 17 59.5401	+25 08 12.616	25	2.51±0.08 ^a
1989.279 ...	VLA	1210	8.4	38	14 17 59.5391	+25 08 12.596	25	2.55±0.09 ^a
1989.318 ...	VLA	1210	8.4	32	14 17 59.5411	+25 08 12.636	25	2.14±0.07 ^a
1992.814 ...	VLA	500	8.4	67	14 17 59.5401	+25 08 12.604	20	2.61±0.10 ^a
1992.814 ...	VLA	500	4.9	76	14 17 59.5406	+25 08 12.594	20	2.94±0.12 ^a
1992.858 ...	VLA	500	8.4	66	14 17 59.5395	+25 08 12.608	20	2.74±0.11 ^a
1992.858 ...	VLA	500	4.9	96	14 17 59.5388	+25 08 12.600	20	3.03±0.13 ^a
1992.891 ...	VLA	500	8.4	56	14 17 59.5402	+25 08 12.613	20	2.67±0.10 ^a
1992.891 ...	VLA	500	4.9	105	14 17 59.5406	+25 08 12.603	20	2.95±0.14 ^a
1992.997 ...	VLA	500	8.4	50	14 17 59.5396	+25 08 12.598	20	2.72±0.10 ^a
1992.997 ...	VLA	500	4.9	78	14 17 59.5413	+25 08 12.600	20	3.07±0.12 ^a
1993.025 ...	VLA	500	8.4	69	14 17 59.5397	+25 08 12.596	20	2.79±0.11 ^a
1993.025 ...	VLA	500	4.9	111	14 17 59.5396	+25 08 12.602	20	3.08±0.14 ^a
1993.162 ...	VLA	1210	8.4	49	14 17 59.5400	+25 08 12.603	25	4.28±0.14 ^a
1993.162 ...	VLA	1210	4.9	64	14 17 59.5400	+25 08 12.603	25	3.74±0.13 ^a
1993.203 ...	VLA	1210	8.4	47	14 17 59.5380	+25 08 12.653	25	4.29±0.14 ^a
1993.203 ...	VLA	1210	4.9	68	14 17 59.5390	+25 08 12.593	25	3.88±0.14 ^a
1993.249 ...	VLA	1210	8.4	47	14 17 59.5410	+25 08 12.613	25	4.84±0.15 ^a
1993.249 ...	VLA	1210	4.9	65	14 17 59.5390	+25 08 12.603	25	4.00±0.14 ^a
1993.277 ...	VLA	1210	8.4	43	14 17 59.5400	+25 08 12.603	25	5.26±0.16 ^a
1993.277 ...	VLA	1210	4.9	64	14 17 59.5400	+25 08 12.603	25	4.38±0.15 ^a
1993.315 ...	VLA	1210	8.4	46	14 17 59.5390	+25 08 12.623	25	5.72±0.18 ^a
1993.315 ...	VLA	1210	4.9	62	14 17 59.5390	+25 08 12.623	25	4.60±0.15 ^a
1995.337 ...	VLBA	2.3,1.1,−6°	8.4	92	14 17 59.53973	+25 08 12.6048	1.3	2.40±0.30 ^b
1998.445 ...	VLBA	2.3,1.1,−6°	8.4	55	14 17 59.53972	+25 08 12.6049	1.3	1.70±0.20 ^b
1998.481 ...	VLBA	2.3,1.1,−6°	8.4	58	14 17 59.53972	+25 08 12.6053	1.3	1.70±0.20 ^b

^aPeak in mJy ba^{−1}.

^bTotal in mJy from areal integration.